Biochimica et Biophysica Acta 1850 (2015) 1426–1437

Contents lists available at ScienceDirect

Biochimica et Biophysica Acta

journal homepage: www.elsevier.com/locate/bbagen

Expression in yeast, new substrates, and construction of a first 3D model of human orphan cytochrome P450 2U1: Interpretation of substrate hydroxylation regioselectivity from docking studies

Lionel Ducassou [a], Gabriella Jonasson [b], Laura Dhers [a], Nicolas Pietrancosta [a], Booma Ramassamy [a], Yun Xu-Li [a,1], Marie-Anne Loriot [c], Philippe Beaune [c], Gildas Bertho [a], Murielle Lombard [a,1], Daniel Mansuy [a], François André [b,*], Jean-Luc Boucher [a,**]

[a] UMR 8601 CNRS, University Paris Descartes, Paris Sorbonne Cité, 75270 Paris, France.
[b] UMR 9198 CNRS, University Paris Sud, iBiTec-S/SB2SM, CEA Saclay, 91191 Gif sur Yvette, France
[c] UMR S 775 INSERM, University Paris Descartes, Paris Sorbonne Cité, 75270 Paris, France

ARTICLE INFO

Article history:
Received 5 January 2015
Received in revised form 23 March 2015
Accepted 30 March 2015
Available online 7 April 2015

Keywords:
Orphan cytochrome P450
Expression in yeast
Debrisoquine
Terfenadone analogue
Active site topology
Docking experiment

ABSTRACT

Background: Cytochrome P450 2U1 (CYP2U1) has been identified from the human genome and is highly conserved in the living kingdom. In humans, it has been found to be predominantly expressed in the thymus and in the brain. CYP2U1 is considered as an "orphan" enzyme as few data are available on its physiological function(s) and active site topology. Its only substrates reported so far were unsaturated fatty acids such as arachidonic acid, and, much more recently, *N*-arachidonoylserotonin.
Methods: We expressed CYP2U1 in yeast *Saccharomyces cerevisiae*, built a 3D homology model of CYP2U1, screened a library of compounds known to be substrates of CYP2 family with metabolite detection by high performance liquid chromatography–mass spectrometry, and performed docking experiments to explain the observed regioselectivity of the reactions.
Results: We show that drug-related compounds, debrisoquine and terfenadine derivatives, subtrates of CYP2D6 and CYP2J2, are hydroxylated by recombinant CYP2U1 with regioselectivities different from those reported for CYP2D6 and 2J2. Docking experiments of those compounds and of arachidonic acid allow us to explain the regioselectivity of the hydroxylations on the basis of their interactions with key residues of CYP2U1 active site.
Major conclusion: Our results show for the first time that human orphan CYP2U1 can oxidize several exogenous molecules including drugs, and describe a first CYP2U1 3D model.
General significance: These results could have consequences for the metabolism of drugs particularly in the brain. The described 3D model should be useful to identify other substrates of CYP2U1 and help in understanding its physiologic roles.

1. Introduction

Cytochromes P450 (CYPs) constitute a superfamily of hemoproteins that play key roles in the metabolism of a large variety of endogenous compounds and xenobiotics [1]. In the human genome, 57 genes have been found to code for CYPs. Among them, about fifteen are known to be involved in the metabolism of xenobiotics and participate in the elimination of exogenous compounds such as drugs, toxins or pollutants, and about thirty human CYPs are involved in the biosynthesis of endogenous compounds such as sterols, vitamins and eicosanoids [2]. Very few data are presently available for the other human CYPs that have been recently discovered from an analysis of the human genome, and the CYPs whose biological roles and functions remain poorly known are called "orphan CYPs" [2–4].

Among them, CYP2U1 displays high sequence homology with CYP2R1, 2D6, and 2J2, and is highly conserved among the living kingdom

Abbreviations: AA, arachidonic acid; a.m.u., atomic mass unit; a.u., arbitrary units; CYP, cytochrome P450; Deb, debrisoquine; 1- 3-, 4-, 5-, 6-, 7- and 8-OH-Deb, 1-, 3-, 4-, 5-, 6-, 7-, and 8-hydroxy-debrisoquine, respectively; *N*-OH-Deb, *N*-hydroxy-debrisoquine; Deb-urea, urea derivative of debrisoquine; Et-Terf, ethyl-terfenadone; ESI, electrospray ionization; HETE, hydroxy-eicosatetraenoic acid; HMQC, heteronuclear multiple-quantum correlation; MD, molecular dynamics; MS/MS, tandem mass spectrometry; NOESY, nuclear Overhauser effect spectroscopy; RMSD, root mean square deviation; Rt, retention time; SAMS, solvent accessible molecular surface; Terf, terfenadone; TOCSY, total correlation spectroscopy

* Correspondence author. Tel.: +33 1 69 08 44 32; fax: +33 1 69 08 87 17.
** Correspondence to: J.-L. Boucher, UMR8601 CNRS, University Paris Descartes, 45 rue des Saints Pères, 75270 Paris, cedex 06, France. Tel.: +33 1 42 86 21 91; fax: +33 1 42 86 83 87.
E-mail addresses: francois.andre@cea.fr (F. André), jean-luc.boucher@parisdescartes.fr (J.-L. Boucher).
[1] Present address: Laboratoire de Chimie des Processus Biologiques, Collège de France, 75231 Paris, France.

http://dx.doi.org/10.1016/j.bbagen.2015.03.014
0304-4165/

[5–8]. Studies of the distribution of CYP2U1 mRNA and protein have shown that it is preferentially expressed in the thymus and cerebellum; its presence was also detected in the kidneys, lungs, heart, white adipose tissue, platelets, and the blood–brain barrier [5,6,9–15]. CYP2U1 was found to be up-regulated in a variety of cancer tissues such as breast or colorectal cancer tissues [16,17]. Very recently, mutations in the CYP2U1 gene were found to be related to the appearance of hereditary spastic paraplegia, a neurological disorder [18]. Other data have shown that CYP2U1 catalyzes the hydroxylation of some polyunsaturated fatty acids [6]. In the case of arachidonic acid (AA), the CYP2U1-dependent hydroxylation was found to occur in ω- and ω-1 positions [6]. Moreover, during the preparation of this manuscript, it was reported that CYP2U1 also catalyzed the oxidation of N-arachidonoylserotonin at position 2 of its indole ring [19]. However, the precise biological roles of CYP2U1, its ability to oxidize xenobiotics, and its structure remain so far unknown.

In order to find other possible CYP2U1 substrates, including drugs, and to get a first idea of the 3D structure of this protein, we have expressed CYP2U1 in yeast *Saccharomyces cerevisiae* co-expressing human cytochrome P450 reductase W(hR), and constructed a 3D homology model of CYP2U1. Docking of AA in the active site of this model allowed us to explain the unusual hydroxylation regioselectivity previously reported for this substrate [6], which gave a first validation of the model. Then, in order to find new CYP2U1 substrates and to know if CYP2U1 could be involved in drug metabolism, the ability of CYP2U1-expressing yeast microsomes to oxidize a library of molecules was tested, with a special focus on compounds known to be substrates of CYP2 family members. This led us to find first xenobiotic CYP2U1 substrates: debrisoquine (Deb) (Scheme 1), an anti-hypertensive drug [20] which is a well-known substrate of CYP2D6 [21,22], and some analogues of terfenadine (Terf) (Scheme 2), an antihistaminic drug known to be a substrate of CYP3A4 and CYP2J2 [23–26]. The regioselectivity of these CYP2U1-dependent oxidations greatly differed from those catalyzed by CYP2D6 and CYP2J2. Noticeably, this regioselectivity could be explained by docking experiments of Deb and Terf in our rebuilt structural 3D model of CYP2U1.

2. Materials and methods

2.1. Chemicals

Most chemicals and biochemicals were purchased from Sigma-Aldrich (Saint-Quentin Fallavier, France), Alfa-Aesar (Schiltigheim, France) or Difco Laboratories (COGER, Paris, France). All organic solvents were purchased from SDS (Peypin, France) and were of the highest purity available. [1-^{14}C]Arachidonic acid (sp. act, 50 mCi/mmol) was provided by Perkin-Elmer (Courtaboeuf, France). Ebastine came from Pharmafarm (Paris, France), and 4-hydroxy-debrisoquine (4-OH-Deb) and 8-hydroxy-debrisoquine (8-OH-Deb) from Toronto Research Chemicals (Toronto, Canada). 4-[4-(Hydroxydiphenylmethyl)piperidin-1-yl]-1-(4-*tert*-butylphenyl)butan-1-one (terfenadone), 4-[4-(hydroxydiphenylmethyl)piperidin-1-yl]-1-(4-methylphenyl)butan-1-one (methyl-terfenadone), **7**, 4-[4-(hydroxydiphenylmethyl)piperidin-1-yl]-1-(4-ethylphenyl)butan-1-one (ethyl-terfenadone, Et-Terf), **8**, 4-[4-(hydroxydiphenylmethyl)piperidin-1-yl]-1-(4-propylphenyl)butan-1-one (propyl-terfenadone), **9**, 4-[4-(hydroxydiphenylmethyl)piperidin-1-yl]-1-(4-butylphenyl) butan-1-one (butyl-terfenadone), **10**, 4-[4-(hydroxydiphenylmethyl)piperidin-1-yl]-1-[4-(3-hydroxypropyl)phenyl]butan-1-one, **11**, and, 3-({4-[4-(hydroxydiphenylmethyl)piperidin-1-yl]-1-oxobutyl}phenyl)propyl acetate, **12**, were synthesized as described previously [24–26]. Benzylguanidine, **4**, 2-phenyl-ethylguanidine, **5**, and 6,7-dimethoxy-1,2,3,4-tetrahydro-*iso*-quinoline carboxamidine, **6**, were prepared by reaction of the corresponding amines with di-Boc-*1H*-pyrazole-1-carboxamidine followed by HCl deprotection of the guanidine [27]. Synthesis and characterization of authentic Deb metabolites and Deb analogues **4–6** are detailed in the Supporting information. All authentic Deb metabolites were fully characterized by UV–vis, ^{1}H NMR and mass spectroscopy (see Supporting information). Their ^{1}H NMR and MS spectra were in accordance with previously described data [28].

2.2. Origins of recombinant CYPs

Microsomes from baculovirus-infected *Spodoptera frugiperda* insect cells coexpressing one of the following CYPs (CYP1A2, CYP2A6, CYP2C9, CYP2C19, CYP2D1, CYP2D6, CYP2E1, CYP2R1 or CYP3A4) with CYP reductase (Supersomes®) were purchased from BD Biosciences (Le Pont de Claix, France). CYP2J2 with the human CYP reductase and cytochrome *b5* over-expressed in *Escherichia coli* (Bactosomes®) was provided by Cypex (Dundee, UK).

Preparation of full-length cDNA of *cyp2u1*, expression of CYP2U1 in several strains of yeast *S. cerevisiae*, electrophoresis and western blot analysis for CYP2U1 were performed following usual procedures [29–31] and are detailed in the Supporting information. The protein concentrations were measured by the Bradford method using bovine serum albumin as a standard [32]. The CYP concentrations were measured on a Cary300 spectrophotometer (Varian, Les Ulis, France) by UV–visible difference spectroscopy of the Fe^{II}–CO complexes using an ε value of 91,000 $M^{-1} \cdot cm^{-1}$ [33]. The cytochrome *c* reductase activity of yeast microsomes was measured by monitoring the absorbance at 550 nm at 25 °C and using a Δε value of 21,000 $M^{-1} \cdot cm^{-1}$ [33].

2.3. Search for substrates and identification of metabolites

2.3.1. Oxidation of arachidonic acid by yeast microsomes expressing CYP2U1

The ability of microsomes from W(hR) yeast expressing CYP2U1 to hydroxylate AA was studied after incubation of microsomes containing 0.1 nmol CYP2U1 in 0.1 M phosphate buffer pH 7.4, in the presence of 1 mM EDTA, 5 mM $MgCl_2$, and 30 μM [1-^{14}C]arachidonic acid in a final volume of 50 μL. Incubation mixtures containing all of the reagents except NADPH were incubated for 5 min at room temperature, then

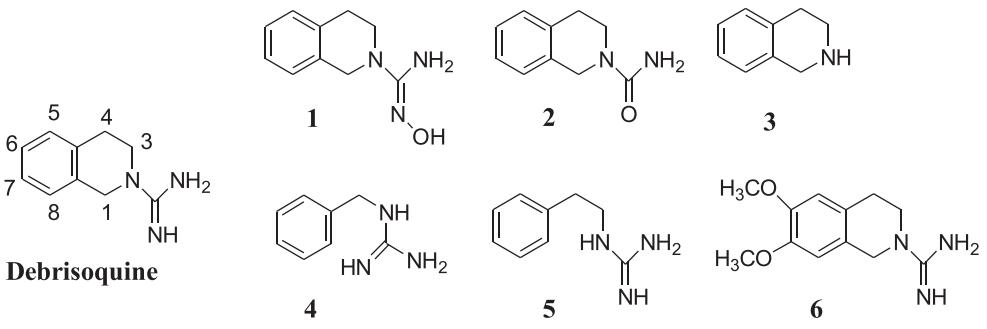

Scheme 1. Structure of Deb with numbering of its C-atoms, and structure of the Deb analogues **1–6** evaluated as substrates of yeast microsomes expressing CYP2U1.

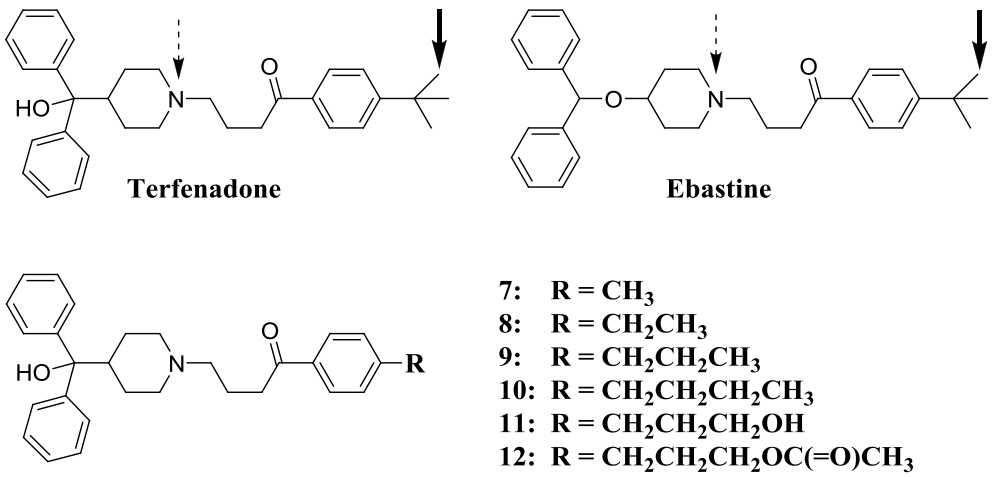

Scheme 2. Structure of Terf, ebastine, and Terf analogues **7–12** tested as substrates of recombinant CYP2U1. Black arrows show the major site of hydroxylation of Terf and ebastine by CYP2J2 and dashed arrows by CYP3A4.

2 min at 28 °C before initiation of the reactions with 1 mM NADPH. After 1 h at 28 °C, the reactions were stopped by addition of 25 μL cold acetonitrile/acetic acid mixture (10:1, v/v), and centrifugation at 5000 *g* for 10 min. The metabolites were separated by HPLC on a Spectra Physics system (Thermo, Les Ulis, France), using a Zorbax C18 Elipse XDB 150 × 2.1 mm, 5-μm particle size (AIT France, Houilles, France) analytical column. Separation was achieved using a gradient between solvent A (water + 0.1% acetic acid) and solvent B (acetonitrile + 0.1% acetic acid) at a flow rate of 0.4 mL · min^{-1} under the following conditions: 30% B for 2 min, then linear increase to 100% B in 35 min, isocratic elution at 100% B for 3 min before returning to the initial conditions and equilibrating for 10 min. Fractions were collected each 0.5 min, mixed with PicoFluor 40 (Perkin-Elmer, Courtaboeuf, France), and radioactivity contained in each vial was measured on a TriCarb 2100 scintillation counter (Perkin-Elmer). Retention time for 19- and 20-hydroxy-eicosatetraenoic acid (HETE) (as bulk) was 14.0 ± 0.5 min.

2.3.2. Usual incubation conditions for the screening of potential substrates of CYP2U1 and HPLC-MS analysis

Usual incubations (total volume 200 μL) contained 0.2 nmol CYP2U1 in 0.1 M phosphate buffer pH 7.4, in the presence of 1 mM EDTA, 5 mM $MgCl_2$, and 0.2 mM of the studied compound diluted in a suitable solvent (organic solvent < 2% of the final volume). Following a 2 min pre-incubation, the reactions were started by addition of NADPH (1 mM, final concentration). Incubations were performed at 28 °C with yeast microsomes (37 °C otherwise) for 1 h, and stopped by the addition of 100 μL of a cold mixture of acetonitrile/acetic acid (10:1 v/v). Control experiments were carried out under identical conditions but without NADPH or with microsomes from W(hR) yeast not expressing CYP2U1. Reaction mixtures were centrifuged (5000 *g*, 10 min) to precipitate the proteins. Aliquots of the supernatants were injected, separated and analyzed on a Surveyor HPLC system coupled to a LCQ Advantage ion trap mass spectrometer (Thermo). HPLC separations were usually achieved on a Gemini C18 column (100 × 2 mm, 3 μm; Phenomenex, Le Pecq, France). Elution (flow rate 200 μL/min) was performed using a mixture of solvent A (10 mM ammonium acetate, pH 4.6) and B (acetonitrile/methanol/water, 7:2:1 v/v). The gradient and mass spectra conditions were adapted for each of the studied compounds. The column effluents were directed to the ion source 3 min after injection to reduce contamination. Mass spectra were recorded in the positive or negative electrospray ionization modes (ESI^+ or ESI^-) with a resolution of approximately 1 atomic mass unit (a.m.u.). HPLC-MS chromatograms and UV–Vis spectra were analyzed with Excalibur software (Thermo).

2.3.3. Oxidation of debrisoquine and Deb analogues by CYP2U1

For kinetic determinations, the incubation time was 20 min; CYP2U1 concentration was 1 μM, and NADPH 1 mM. Eight concentrations were examined in the 100 μM–5 mM range. Aliquots of the incubations were analyzed on a Gemini C18 column (100 × 2 mm, 3 μm, Phenomenex) with the following gradient conditions: 100% solvent A (10 mM ammonium acetate, pH 4.6) for 5 min, linear gradient to 25% B (acetonitrile/methanol/water, 7:2:1 v/v) in 15 min, linear gradient to 100% B in 1 min, holding at 100% B for 4 min, returning to 100% A in 1 min, and re-equilibration at 100% A for 10 min. Flow rate was 200 μL/min. Mass spectra were obtained by ESI in positive detection mode under the following conditions: capillary temperature, 200 °C; capillary voltage, 15 V; spray voltage, 4.5 kV; primary gas flow, 20 arbitrary units (a.u.); auxiliary gas flow, 5 a.u. MS/MS energy was tested between 20 a.u. and 40 a.u. Analysis and quantification of Deb and its metabolites were performed by integration of reconstructed ion-current chromatograms of the protonated molecular ions of interest and calibration curves obtained with 4-OH-Deb. The range of masses scanned for the total-ion chromatogram was *m/z* 100–500 a.m.u. For all products, the indicated molecular ions corresponded to $M + H^+$ (Deb, *m/z* 176, and OH-Deb, *m/z* 192).

2.3.4. Characterization of Deb metabolite M3

This metabolite was obtained from large scale incubations and purified by HPLC on a semi-preparative X-Bridge Prep Shield RP18 column (250 × 10 mm, 5 μm; Waters, Saint Quentin en Yvelines, France). Elution (flow rate 2 mL/min) was performed using a mixture of solvent A (10 mM ammonium acetate, pH 4.6) and B (acetonitrile/methanol/water, 7:2:1 v/v) with the following gradient conditions: 0% B for 5 min, linear gradient to 25% B in 15 min, linear gradient to 100% B in 1 min, holding at 100% B for 4 min, returning to 0% B in 1 min, and re-equilibration at 0% B for 10 min. The absorption at 260 nm was monitored and fractions containing metabolite M3 were pooled and concentrated. The residue was dissolved in D_2O and analyzed by ^1H NMR. Assignments of all the signals were made by 2D-NMR experiments (TOCSY, HMQC and NOESY, see Fig. S2 of the Supporting information) on a Bruker Avance 500 MHz spectrometer. These experiments indicated that metabolite M3 was a mixture of two isomers (**M3a** and **M3b**) of 1-hydroxy-debrisoquine in equilibrium in a 1:1 ratio that differ by the presence (or absence) of a hydrogen bond between the alcohol and guanidine functions, and flipping of the 6-atom ring. Molecular modeling of these isomers suggested that their difference in energy would be of 1.5 kJ·mol^{-1} only, in agreement with the 1:1 ratio observed in ^1H

NMR. **M3a**: ^{1}H NMR (D_2O, 500 MHz) δ = 3.04 (m, H_4), 3.12 (m, $H_{4'}$), 3.54 (d, $2H_3$, J = 6.7), 5.87 (s, H_1), 7.34 (d, H_5, J = 8.0), 7.39 (dd, H_7, J = 7.5 and 2.0), 7.41 (dd, H_6, J = 7.5 and 2.0), and 7.56 (dd, H_8, J = 7.5 and 1.7); ^{13}C NMR (D_2O, 125 MHz) δ = 31.1 (C_4), 42.0 (C_3), 63.1 (C_1), 125.6 (C_8), 127.8 (C_7), 128.1 (C_6), and 128.5 (C_5). **M3b**: ^{1}H NMR (D_2O, 500 MHz) δ = 2.97 (m, H_4), 3.13 (m, $H_{4'}$), 3.59 (m, H_3), 3.80 (dd, $H_{3'}$), 5.94 (s, H_1), 7.29–7.32 (m, H_5 + H_6 + H_7), and 7.45 (d, H_8, J = 7.5); ^{13}C NMR (D_2O, 125 MHz) δ = 27.4 (C_4), 42.0 (C_3), 67.9 (C_1), 125.7 (C_8), 126.9 (C_7), 128.1 (C_6), and 128.3 (C_5).

2.3.5. Oxidation of terfenadone analogues by CYP2U1

For kinetic determinations, the incubation time was 20 min; CYP2U1 concentration was 1 μM and NADPH 1 mM. Eight concentrations were examined in the 200 μM–5 mM range. The column was a Gemini C18 column (100 × 2 mm, 3 μm, Phenomenex) with the following gradient conditions: 70% solvent A (10 mM ammonium acetate, pH 4.6) for 5 min, linear gradient to 100% B (acetonitrile/methanol/water, 7:2:1 v/v) in 15 min, holding at 100% B for 4 min, returning to 100% A in 1 min, and re-equilibration at 100% A for 10 min. Flow rate was 200 μL/min. Elution was monitored at 254 nm for quantification. MS were obtained using an ESI source in positive mode with a capillary temperature of 275 °C, a capillary voltage of 40 V, and a spray voltage of 5 kV.

2.4. Computational

All computations were performed on a Dell Precision Workstation connected to the Computing Center for Research and Technology (CCRT, Bruyère-le-Châtel, France).

A 3D model of CYP2U1 deprived of its membrane spanning domain (residues 57 to 544, Fig. S4 of the Supporting information) was built using Modeller9v8 [34] and the crystal structures of CYP2D6 (PDB ID: 2F9Q), CYP2R1 (PDB ID: 3CZH), CYP2A6 (PDB ID: 1Z10), CYP2C5 (PDB ID: 1DT6), CYP2B4 (PDB ID: 1PO5) and CYP2C8 (PDB ID: 1PQ2) as templates. The validated sequence alignment used as input for Modeller is shown in Fig. S5 of the Supporting information. 500 models were generated and evaluated by their DOPE (Discrete Optimized Protein Energy) and GA341 scores calculated by Modeller. Validation of the protein structures was applied at this early stage to the five best models (corresponding to the lowest DOPE scores) by using PROCHECK [35], WHAT_CHECK [36], ERRAT [37] and VERIFY_3D [38] as proposed by the Structural Analysis and Verification Server (http://services.mbi.ucla.edu/SAVES). The final model was the best one according to a good compromise between the score calculated by the four programs.

Optimization of the 3D model was done by several cycles of minimization and molecular dynamics (MD) simulations (20 ns runs) using the AMBER ff99 force field parameters [39]. Bonds involving hydrogen atoms were constrained by using the SHAKE algorithm [39]. At the end of each optimization, the final structure was controlled using PROCHECK and VERIFY_3D [35,38]. In all modeling experiments, the parameters applied for the heme (defined as Fe^{III} protoporphyrin IX) were obtained from Oda et al. [40], except in the docking experiments of AA in the CYP2U1 model, that were performed more recently and in which the heme was defined as the highly reactive intermediate compound I (Fe^{IV} = O)$^{+\cdot}$ by using the parameters (geometry and atom charges) of an AMBER-compatible heme model recently developed by Shahrokh et al. [41]. Cavity volumes were calculated using VOIDOO software [42] and access/egress channels were analyzed using MOLE 1.4 installed package (http://mole.chemi.muni.cz) [43]. Ptraj (AMBER Package) scripting was used to calculate root mean square deviations (RMSDs) and gyration radii during the simulated trajectories.

Molecular docking experiments of AA, Deb and Terf analogues at the active site were performed using AutoDock 4.2 in the flexible mode [44,45]. Docking experiments of AA were also performed using CDOCKER [46] with Discovery Studio 4.1 (Accelrys, Dassault Systems Biovia). The PyMOL Molecular Graphics System, Version 1.4 was used for structure rendering. Detailed procedures for all calculations are given in the Supplementary information.

3. Results and discussion

3.1. Expression in yeast and characterization of CYP2U1

Several yeast *S. cerevisiae* strains transformed by the *pYeDP60-cyp2U1* plasmid to express CYP2U1 and CYP reductase and several culture conditions were tested to optimize the preparation of recombinant CYP2U1. The assays included previously described strain W(R) over-expressing yeast CYP reductase, strain W(hR) over-expressing human CYP reductase, strain W(N) expressing yeast CYP reductase and yeast W(hR) transformed with an empty *pYeDP60* plasmid (as a negative control) [31]. Microsomal fractions containing CYP2U1 were then prepared and their CYP contents and reductase activities were measured. A strong reductase activity was measured for microsomes from strain W(R) (1600 ± 200 nmol·min^{-1}·mg prot^{-1}) whereas the activities of microsomes from W(hR) and W(N) strains were 1200 ± 200, and 60 ± 15 nmol·min^{-1}·mg prot^{-1}, respectively. The CYP contents of each preparation were measured by UV–vis difference spectroscopy of the Fe^{II}–CO complexes. A Fe^{II}–CO difference spectrum with a major absorption peak at 450 nm was only observed for microsomes from the W(hR) strain indicating a CYP2U1 content of 60 ± 22 pmol·mg prot^{-1} (Fig. 1A). By contrast, microsomes from the W(R) strain led to spectra with two peaks at 450 and 420 nm, suggesting that these preparations contained an inactive form of CYP (data not shown). In the following, expression of CYP2U1 was thus carried out in strain W(hR) (~0.8 ± 0.2 nmol CYP2U1/L of culture) and the corresponding microsomes were used for substrate screening. Western-blot analyses confirmed the expression of recombinant CYP2U1 as a band set at ~60 kDa was observed for microsomes from W(hR) yeast expressing CYP2U1 (Fig. 1B, Line 3) whereas this band was absent in microsomes from yeast W(hR) transformed with an empty vector (Fig. 1B, Line 2).

3.2. Oxidation of arachidonic acid by CYP2U1

As CYP2U1 was previously reported to hydroxylate arachidonic acid [6], oxidation of this substrate by microsomes from the W(hR) yeast transformed by the *pYeDP60-cyp2U1* plasmid was studied. Those microsomes were found to be catalytically active for AA hydroxylation (see Materials and methods), whereas microsomes of yeast transformed with an empty plasmid were not. The catalytic activity was low (12 pmol 19- and 20-HETE·min^{-1}·nmol P450^{-1}) but similar to that very recently reported for CYP2U1 expressed in *E. coli* (19.5 pmol·min^{-1}·nmol P450^{-1}) [19].

3.3. Search for new substrates of CYP2U1

In order to find new substrates of CYP2U1, we have tested a series of molecules, most of which were known to be transformed by other members of the CYP2 family. This included known substrates of CYP2J2, 2D6 and 2R1 that are the closest CYPs phylogenetically related to CYP2U1 [5,6]. Activity assays were performed by incubating W(hR) yeast microsomes expressing CYP2U1 and putative substrates in the presence or absence of NADPH. Detection of the hydroxylated metabolites was performed by HPLC-MS searching for products with a m/z ratio increased by 16 a.m.u. relative to the starting compounds. In some cases, we also searched for metabolites that could result from an oxidative demethylation reaction (m/z −14 relative to the starting compound). A library of about forty compounds was tested, including both endogenous and exogenous molecules (Table S1 of the Supporting information). Control incubations in the presence of a CYP isoform known to transform the studied compound were performed to ensure both the validity of the assay and of the detection method. Under our incubation and detection

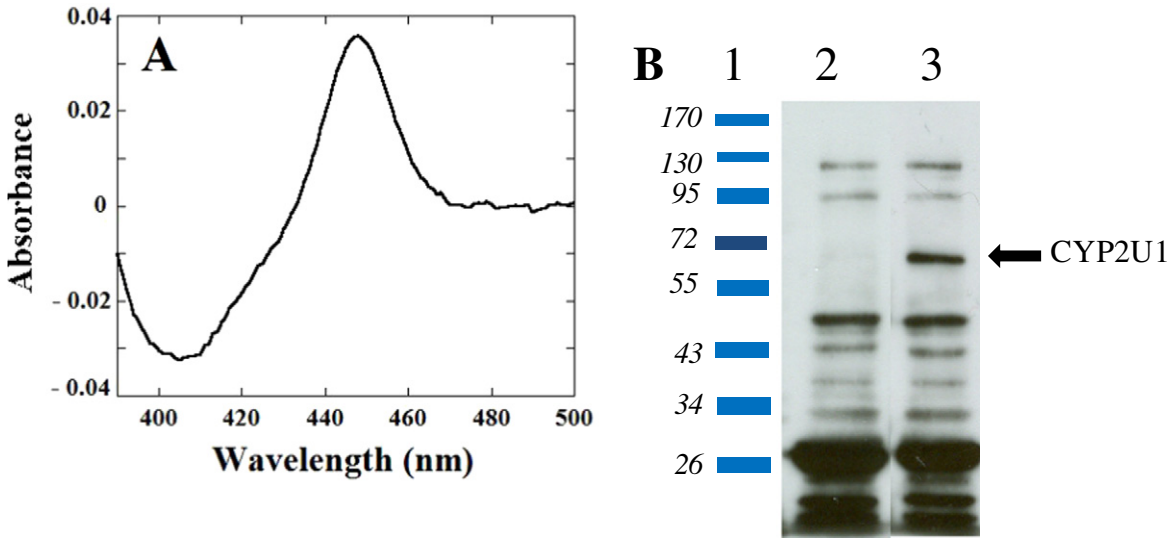

Fig. 1. Characterization of recombinant CYP2U1. A: UV visible difference spectrum of the heme-Fe^{II}–CO complex of microsomes of yeast strain W(hR) expressing CYP2U1. B: Autoradiography of a western blot membrane. Line 1: molecular mass markers. Line 2: microsomes from yeast strain W(hR) transformed with an empty vector. Line 3: microsomes from yeast transformed with plasmid *pYeDP60-cyp2u1*.

conditions, most tested compounds led to levels of CYP2U1-dependent metabolites below our detection limits (estimated to be 0.5 μM). However, we observed significant formation of hydroxylated compounds from two of the studied compounds, Deb and Et-Terf. Keeping in mind the limits of this screening method, these results clearly identified Deb and Et-Terf as substrates of CYP2U1.

3.4. Oxidation of debrisoquine and debrisoquine analogues by CYP2U1

Debrisoquine is known to be oxidized by CYP2D6 into several metabolites. 4-(*S*)-Hydroxy-debrisoquine (4-OH-Deb) is the predominant product [47–49] whereas other metabolites, including phenols (5-, 6-, 7- and 8-OH-Deb) (see Scheme **1** for numbering of atoms) [22], a dehydration product (3,4-dehydro-debrisoquine) [50], and two acids derived from the ring opening of 1- and 3-hydroxy-debrisoquines [51, 52] have been previously identified. Finally, *N*-hydroxy-debrisoquine (N-OH-Deb), and its urea derivative (Deb-urea) have also been reported as Deb metabolites formed by rabbit CYP2C3 [53].

Analysis of the reaction mixtures obtained from incubations of Deb in the presence of NADPH and microsomes of W(hR) yeast expressing CYP2U1 led to the appearance of four new peaks in HPLC-MS with an *m/z* 192: compounds M1 (11 ± 2% of total hydroxylated compounds), M2 (21 ± 2%), M3 (68 ± 2%) and M4 (1–2%) (Fig. S1 of the Supporting information). In the absence of NADPH or in the presence of microsomes of yeast transformed with an empty plasmid, no detectable formation of these metabolites could be observed. Moreover, addition of 1 mM benzyl-imidazole or 100 μM clotrimazole, two known CYP inhibitors [54], led to an almost complete inhibition of the formation of compounds M1–M4 (data not shown). This clearly indicated that the observed metabolites were derived from CYP2U1-catalyzed oxidations. Finally, no metabolite with a molecular ion at *m/z* 208 (carboxylic acids or diols derived from Deb) or at *m/z* 174 (3,4-dehydro-debrisoquine) could be detected in incubations of Deb with NADPH and CYP2U1 expressing yeast microsomes.

Identification of the observed metabolites was performed on the basis of their HPLC retention times (Rt), mass and UV–visible spectra, by comparison with those of authentic samples of commercially available 4- and 8-OH-Deb, and of 5-, 6-, 7- and *N*-OH-Deb, and Deb-urea that were synthesized in our laboratory (see Materials and methods). Metabolite M1 was clearly identified to 4-OH-Deb, M2 to 6-OH-Deb and M4 to 8-OH-Deb whereas metabolite M3 did not correspond to any of our authentic compounds. However, its MS/MS fragmentation pattern and its UV–visible spectrum were very close to those of 4-OH-Deb; this metabolite was thus tentatively assigned to 1- or 3-OH-Deb. The ^{1}H NMR spectrum of metabolite M3 was characterized by the presence of two broad singlets at 5.88 and 5.94 ppm, by complex aromatic patterns between 7.2 and 7.6 ppm and by aliphatic patterns at 2.9 and 3.9 ppm. This ^{1}H NMR spectrum was thus clearly distinct from that of 4-OH-Deb that displays signals at 4.64 and 4.49 ppm (C(1)H_2) and 4.92 ppm (C(4)H–OH) [28], and from that of 3-OH-Deb formed by recombinant CYP2D1 that has been described to display ^{1}H NMR signals at 5.6 (C(3)H–OH), 4.4 (C(1)H_2) and 3.1 (C(4)H_2) ppm [52]. Full assignment of the ^{1}H NMR signals of metabolite M3 was made by TOCSY, HSQC, and NOESY experiments and the chemical shifts, coupling constants and connectivity were consistent with the OH-group occupying position 1. A complete description of the NMR characteristics of this Deb metabolite is shown in Materials and methods and in Fig. S2 of the Supporting information.

Formation of metabolites M1–M3 was linear with time over 20 min, and was linearly dependent upon the concentration of CYP2U1 (in the 0.1–1.0 μM range, data not shown). Metabolite M4 was present in too low amounts to be accurately quantified. K_m values close to 400 μM and k_{cat} values in the 0.2–0.5 min^{-1} range were measured for the formation of metabolites M1, M2 and M3 (Table **1**).

The activity of CYP2U1 was tested on a series of six Deb analogues (Scheme **1**) under identical conditions. However, none of these analogues led to any detectable amounts of hydroxylated product, suggesting that the CYP2U1 activity was quite specific for Deb. The presence of a guanidine moiety (absent in compounds **1–3**), a hydrophobic

Table 1
Predominant metabolites of Deb formed by recombinant CYP2U1 and CYP2D6, and kinetic constants measured for the corresponding hydroxylations.

Enzyme	Metabolite	K_m (μM)	k_{cat} [a]
CYP2U1 [b]	1-OH-Deb	480 ± 20	0.5 ± 0.05
	4-OH-Deb	360 ± 20	0.3 ± 0.05
	6-OH-Deb	470 ± 20	0.2 ± 0.05
CYP2D6 [c]	4-OH-Deb	14.9 ± 0.9	2.1 ± 0.1
	6-OH-Deb	15.2 ± 2.2	1.1 ± 0.06

[a] In $nmol \cdot min^{-1} \cdot nmol\ P450^{-1}$.
[b] Kinetic constants were calculated for the formation of the indicated metabolites upon oxidation of Deb (0.1–5 mM) by W(hR) yeast microsomes expressing recombinant CYP2U1. Incubation conditions are described in Materials and methods. Data are means ± S.D. from 3–5 experiments.
[c] From [22].

aromatic ring and an aliphatic ring (absent in compounds **4** and **5**) seem to be required. Finally, increasing the size of the substrate by addition of two methoxy groups (as in compound **6**) resulted in a loss of CYP2U1 activity.

3.5. Oxidation of terfenadone derivatives by CYP2U1

Terfenadine is a non-sedating antihistaminic drug and terfenadone is the ketone analogue obtained after oxidation of the secondary alcohol function of terfenadine, [24–26]. Several derivatives of Terf (structures shown in Scheme **2**) have been tested as substrates or inhibitors of CYP2J2 [24–26], a CYP isoform close to CYP2U1 [5,6]. CYP2J2 predominantly oxidizes the studied Terf analogues at the homobenzylic carbon of their aliphatic chain (black arrows in Scheme **2**) [26]. These compounds were also metabolized by human CYP3A4 but with predominant *N*-dealkylation reactions (dashed arrows in Scheme **2**) [23,24,55].

In analogy with the studies performed on Deb, control experiments in the presence of CYP inhibitors or in the presence of yeast transformed by an empty vector confirmed the involvement of CYP2U1 in the oxidation of Et-Terf into two metabolites, M′1 (82 ± 5% of total metabolites) and M′2 (18 ± 5%), both characterized by a molecular ion at *m/z* 458 (Fig. S3 of the Supporting information). Identification of metabolites M′1 and M′2 was done on the basis of their Rt, UV–visible spectra and characteristic MS/MS fragments in comparison with those of metabolites formed in incubations performed in the presence of CYP2J2 or CYP3A4 [23,26]. M′1 was thus identified as the benzylic alcohol derivative of Et-Terf, and M′2 as the homobenzylic alcohol.

While all the studied Terf analogues shown in Scheme 2 were substrates of CYP2J2 and 3A4, only compounds **7–10** that involve a linear terminal alkyl chain were substrates of CYP2U1 (Table 2). Indeed, Terf itself, ebastine, an isomer of Terf, and compounds **11** and **12** that contained a terminal alcohol or acetate function were not oxidized by CYP2U1. Identifications of the metabolites of the studied Terf analogues were performed as described above by comparison with metabolites obtained in the presence of CYP2J2 [26]. Whatever the studied analogues, benzylic hydroxylation was always the predominant reaction observed and led to 66–82% of the oxidation products (Table 2). The total amount of the other alcohols was small (about 30% of total metabolites). Kinetic constants for the CYP2U1-dependent benzylic hydroxylation of compounds **7–10** are shown in Table 3.

The most striking results of the above described data were the very different regioselectivities found for CYP2U1- and CYP2D6-dependent oxidation of Deb (major 1-hydroxylation with CYP2U1 instead of 4-hydroxylation with CYP2D6), and of CYP2U1- and CYP2J2-dependent oxidation of Terf derivatives (major benzylic hydroxylation with CYP2U1 instead of homobenzylic hydroxylation with CYP2J2).

Table 3
Kinetic constants measured for the hydroxylation of Terf analogues **7–10** catalyzed by recombinant CYP2U1.[a] See Scheme 2 for structure of compounds.

R =	K_m (mM)	k_{cat} [b]
CH_3 (**7**)	1.6 ± 0.5	0.9 ± 0.3
CH_2–CH_3 (**8**)	1.2 ± 0.3	0.4 ± 0.07
CH_2–CH_2–CH_3 (**9**)	0.8 ± 0.3	0.6 ± 0.3
CH_2–CH_2–CH_2–CH_3 (**10**)	1.1 ± 0.4	0.4 ± 0.12

[a] Kinetic constants were calculated for the formation of the predominant metabolites upon oxidation of the compounds (0.2–5 mM) by W(hR) yeast microsomes expressing recombinant CYP2U1. Incubation conditions are described in Materials and methods. Data are means ± S.D. from 3–4 experiments.
[b] In nmol·min^{-1}·nmol P450^{-1}.

3.6. Construction of a homology model of CYP2U1

A 3D model of CYP2U1 deprived of its membrane spanning domain (residues 57 to 544, Fig. S4 of Supporting information) was constructed by comparative modeling. The detection of the most relevant templates in the PDB was performed based upon the PSI-Blast program [56] results and led to the identification of several potential templates in the PDB for CYP2U1 homology modeling, all belonging to CYP2 family, with uniform sequence identity of 35–40%. Despite this uniformity, the templates differ significantly from each other in their primary sequence, especially in the N-terminal domain, and a multiple template homology modeling approach was favored to include all structural local information, without favoring one specific structure. The comparative modeling program Modeller allows combining information from multiple template structures to automatically build the model on the locally best template. The templates most similar to CYP2U1 were, in decreasing order of sequence identity: CYP2D6, CYP2R1, CYP2A6, CYP2C5/2C8/2C9, and CYP2B4. The six templates finally selected covered the structural diversity of CYP2 subfamily, and included, when available, structures without bound substrate to eliminate bias introduced by induced-fit effects, and with the highest resolution available (see Materials and Methods, and Table S2 of the Supporting information). The selection of the most suitable templates has been validated by the remodeling of one of the six templates (as described in the following), and by the systematic comparison of scoring functions of optimized all-atom models generated by Modeller.

Table 2
Experimentally observed regioselectivity of the hydroxylations catalyzed by CYP2U1 and distances between the aliphatic terminal chain carbons of Terf analogues and heme iron deduced from the docking of these substrates in our CYP2U1 3D model. In the case of butyl-terfenadone **10**, the thick arrow on the scheme shows the predominant site of hydroxylation catalyzed by CYP2U1, and thin arrows, the minor sites.

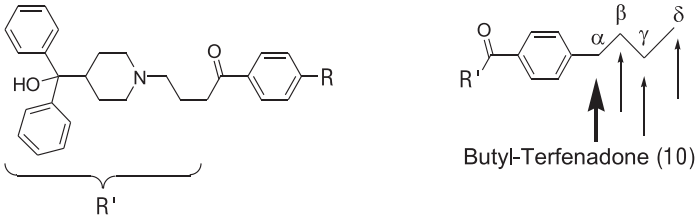

	% Hydroxylation[a]				Distances from the iron[b]			
R =	Cα	Cβ	Cγ	Cδ	Cα	Cβ	Cγ	Cδ
Methyl (**7**)	100				3.6 ± 0.2			
Ethyl (**8**)	82 ± 5	18 ± 5			3.8 ± 0.2	4.9 ± 0.2		
Propyl (**9**)	68 ± 5	22 ± 5	10 ± 2		4.0 ± 0.2	5.3 ± 0.2	6.2 ± 0.4	
Butyl (**10**)	66 ± 5	27 ± 5	7 ± 2	<1	3.5 ± 0.2	4.7 ± 0.2	5.9 ± 0.5	6.7 ± 0.4

[a] % of the regioisomers formed by CYP2U1-dependent hydroxylation of compounds **7–10**. The incubations and metabolite identifications were performed under the conditions described in Materials and Methods. Data are means ± S.D. from 3–4 experiments.
[b] Average distances (in Å) from 10 poses between the considered C-atoms and the iron of CYP2U1 for each of the two clusters of poses.

Several alignment methods have been compared, and two of them have been combined to yield the best consensus alignment. MUSCLE [57] is a well-known multiple alignment method based on primary structure, whereas MUSTANG [58] is based on the multiple alignment of tridimensional structures. MUSTANG was used to superimpose and align the structures of all the known crystal structures of CYPs of family 2. The two multiple alignment approaches were in good agreement (Figs. S4 and S5 of the Supporting information) and a homology model was thus built based on the consensus multiple sequence alignment.

This modeling protocol was validated by the generation of a CYP2D6 test model. CYP2D6 structure file was deleted from the list of templates, and CYP2U1 sequence target replaced by CYP2D6 sequence. A CYP2D6 model was thus generated by Modeller with the five remaining templates. This model was compared to the CYP2D6 crystallographic structure (without substrate, PDB ID: 2F9Q) and an all-atoms RMSD of only 0.89 Å was found. The quality of the CYP2D6 model obtained by this method validated the multiple template alignment of Fig. S5 of the Supporting information.

The final model CYP2U1 structure displayed the best Modeller DOPE score of −61,537. The five best models of CYP2U1 were assessed for both geometric and energetic aspects using the Structural Analysis and Verification Server (http://services.mbi.ucla.edu/SAVES). The PROCHECK evaluation [35] for good stereochemistry of the refined models resulted in 90.5% of the residues in the most favored regions. By comparison, this percentage varied from 85 to 94% for the template structures. VERIFY_3D analysis indicated a good quality of the models with about 88.5% of residues with a score over 0.2. The best scored structures of the model were then solvated and optimized by MD simulation (20 ns) using AMBER [39]. The RMSD observed between the initial model and the last MD pose were 2.1 Å for all atoms, indicating that no protein unfolding occurred during the dynamics. The initial and optimized models were superimposable in their common sequence with an all-atom RMSD of 2.2 Å. After examination of the CYP2U1 model and consideration of previously published works on substrate access channels of mammalian CYPs [59,60], several possible access channels were found for CYP2U1 (Table S3 of the Supporting information) and corresponded to access channels previously identified in several mammalian CYPs [59,60].

3.7. Topology of the CYP2U1 active site

Fig. 2 shows two views of the CYP2U1 active site. The active site cavity is bordered by helices A, F and I, the BC and Kβ1 loops, and the β4-sheet (see also Table S3 of the Supporting information). The CYP2U1 active site volume was calculated according to the VOIDOO program that provides two values corresponding to volumes inside the solvent accessible surface or to the solvent accessible molecular surface (SAMS). The SAMS active site volume of CYP2U1 has been calculated and compared with those of several CYPs for which X-ray structures have been published (Table S4 of the Supporting information). The active site volume of CYP2U1 (931 $Å^3$) was intermediate between those of CYP2E1, 2A6, and 2B4 (<500 $Å^3$), that are known to only admit small substrates, and those of CYPs admitting large substrates (between 1000 and 2000 $Å^3$), such as CYP2C8 [61]. Its volume was comparable to those of CYP2B6, 2C5, or 2J2 (Table S4 of the Supporting information).

3.8. Docking of arachidonic acid in the active site of CYP2U1

Docking calculations were performed using two protocols, Autodock 4.2 and CDOCKER. In order to take account for target structure flexibility, AA was docked in 10 different structures generated directly by the model building program Modeller and in 5 different structures taken from the MD simulation (20 ns). Interestingly, both protocols led to the conclusion that the most energetically favored docking poses were those with AA in a completely extended conformation, stretching through channel 2ac all the way to the protein surface (Fig. 3). In all these poses, the charged carboxyl group of AA interacted with Lys292 at the entrance of channel 2ac (distance between the Lys N^{ε}-atom and an AA O-atom of about 2.9 Å, Fig. 3) and the alkyl chain of AA established hydrophobic interactions with hydrophobic residues all along channel 2ac such as Phe167, Ala352 and Leu530. All these docking poses placed the ω and ω-1 carbons of AA between 2.5 and 3.5 Å from the oxygen atom of the heme iron-oxo group. These distances are in good agreement with the previously reported regioselectivity of CYP2U1-catalyzed AA hydroxylation [6].

3.9. Docking of Deb in the active site of CYP2U1

The positioning of Deb within the active site of CYP2D6 has been extensively studied using several homology models, molecular docking experiments and site directed mutagenesis [62–68]. These data showed that Deb establishes H-bonds between its guanidine moiety and an aspartic acid of helix I (Asp301) and a glutamate (Glu216) of helix F, and hydrophobic interactions with phenylalanine residues (Phe120 and Phe483) [62–68]. Recently, crystallographic studies (PDB ID: 2F9Q and PDB ID: 3QM4) have led to the complete identification of the key amino acid residues involved in substrate binding within the active site of CYP2D6 [69,70]. Alignment and comparison of the F and I helices

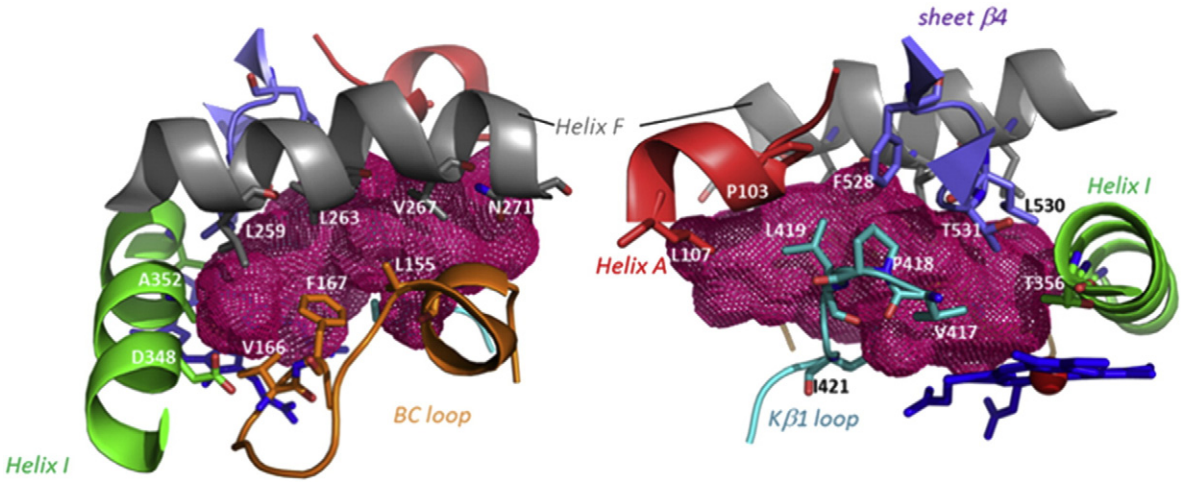

Fig. 2. Active site topology of CYP2U1. Two views of the active site SAMS. CYP2U1 structure is represented in new cartoon. Portions of the structural elements of protein surrounding the active site are shown in red (helix A), gray (helix F), green (helix I), orange (BC loop), cyan (Kβ1 loop) and blue (β4 sheet). The residues bordering the cavity and heme are shown in sticks. The active site cavity surface is rendered with a pink mesh calculated using VOIDOO.

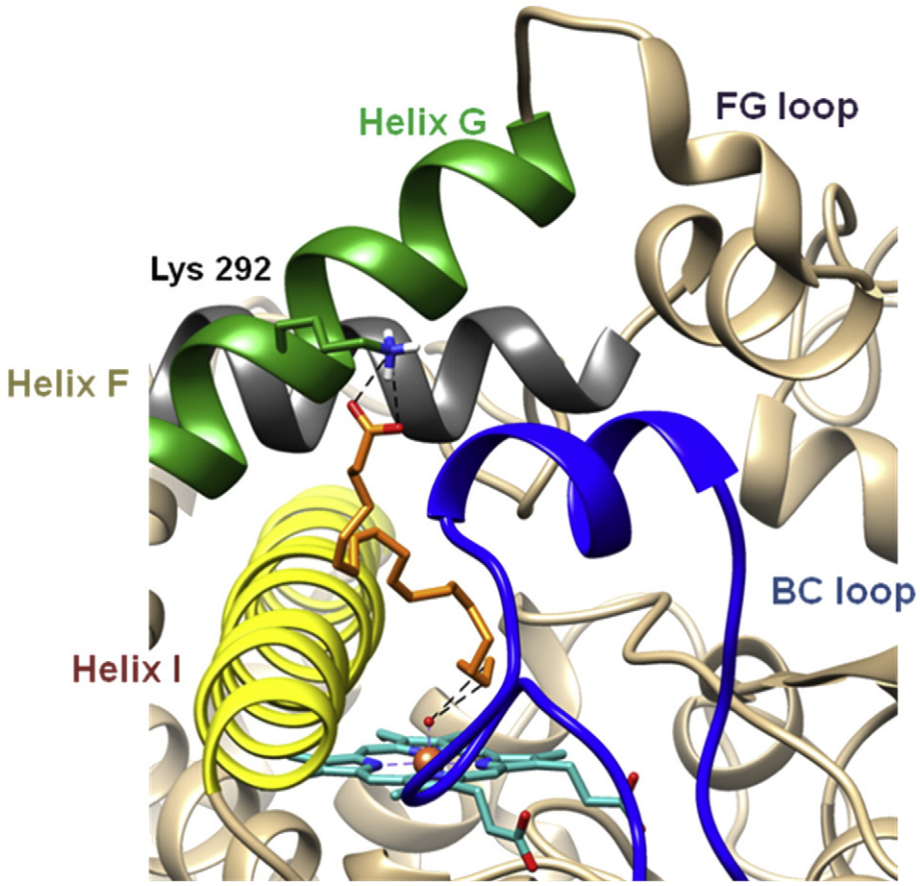

Fig. 3. Docking of AA in CYP2U1. The pose with the best Autodock score is represented in the overall view showing AA (in orange) elongated in access channel 2ac from the heme to the protein surface. On this pose, the ω- and (ω-1)-C-atoms of AA are positioned at 3.39 and 2.90 Å, respectively, from the O-atom of the iron-oxo species, and its carboxyl group is bound to Lys292 at the channel entry (measured distances: 2.94 and 2.98 Å between the O-atoms of AA and the N^{ε}-atom of Lys292).

sequences of CYP2U1 and 2D6 (Fig. S6 of the Supporting information) showed that there was no equivalent of Glu216 of CYP2D6 helix F in CYP2U1. Another glutamate residue (Glu260) was found in CYP2U1 helix F but too far from the active site. Asp301 of CYPD6 helix I has its equivalent in CYP2U1 (Asp348) and there is another aspartic acid residue on helix I of CYP2U1 (Asp355) which is oriented towards the active site. This Asp355 has no counterpart (Asp or Glu) in CYP2D6. Thus, only one of the two key residues that interact with Deb in the active site of CYP2D6 was found in CYP2U1.

As docking calculations in AutoDock are actually limited to a maximum of 32 torsional degrees of freedom in the protein–ligand couple, only residues of the protein that could be in interaction with the substrate were declared flexible and were those identified as possibly lining the active site of CYP2U1. They include Asp348 (equivalent to Asp301 in CYP2D6). The method was validated with the study of the interaction of Deb with CYP2D6 (PDB ID: 2F9Q) with flexible residues including Glu216, Asp301, and residues lining the active site. Our docking experiments led to positions very similar to those published by Rowland et al. with Glu216 forming a salt-link with the guanidine function of Deb and π-stacking interactions with phenylalanine residues [69]. With CYP2U1, the obtained poses (1000) were grouped into clusters; two poses were considered to be close when the calculated RMSD was less than 1.5 Å, and the clusters were ranked as a function of their energy. In all clusters, Deb was found in the active site and it was necessary to check the most energetically favored ones. The first two clusters were composed of about twenty poses, each corresponding to a similar position of Deb within the active site and only differed by a slight translation of Deb in the active site. In one of these two clusters of poses (Fig. 4A), Deb was positioned above the heme plane and stabilized by hydrophobic interactions between the phenyl ring of Deb and hydrophobic residues (Leu530, Val166, Phe167) that surround the active site, and a H-bond between the guanidine function of Deb and a carbonyl group of Leu419 of loop Kβ1. In these two clusters, the closest carbon atom of Deb to the heme iron was carbon-6 with a C(6)–Fe distance of 4.0 Å. In the third cluster of poses (Fig. 4B), Deb established two H-bonds between its guanidine function and the carboxylate group of Asp355 and the carbonyl group of Ile351 of helix I. Furthermore, the aromatic ring of Deb was stabilized by hydrophobic interactions with several hydrophobic residues of the active site (including Phe167). In this third cluster, C(1) of Deb was in close proximity of the iron with a C(1)–Fe distance of 4.3 Å. It was noteworthy that C(4) of Deb also remained in close proximity to the iron with a distance of 4.7 Å whereas C(3) was far away (5.6 Å). This study of the energetically favored clusters of poses was in agreement with the regioselectivity observed for the hydroxylation of Deb catalyzed by CYP2U1. The first two clusters were consistent with an aromatic hydroxylation at C(6) of Deb whereas the third cluster explained the experimentally observed regioselectivity for position-1 of Deb. In this cluster, position-1 was the most energetically favored, and position-3 seemed too far from the iron to be hydroxylated.

3.10. Docking of Terf derivatives in the CYP2U1 active site

Docking of compounds **7–10** in the active site of CYP2J2 has been previously performed using a constrained dynamics method and via a classical semi-flexible method [26,71]. Whatever the method used and irrespective of the studied derivatives, all poses were similar, with the substrate inserted into one of the access channel (2b, according to [59]) and a residue of the BC loop, Arg117, playing a key role by establishing a H-bond interaction with the carbonyl group of Terf [26,71].

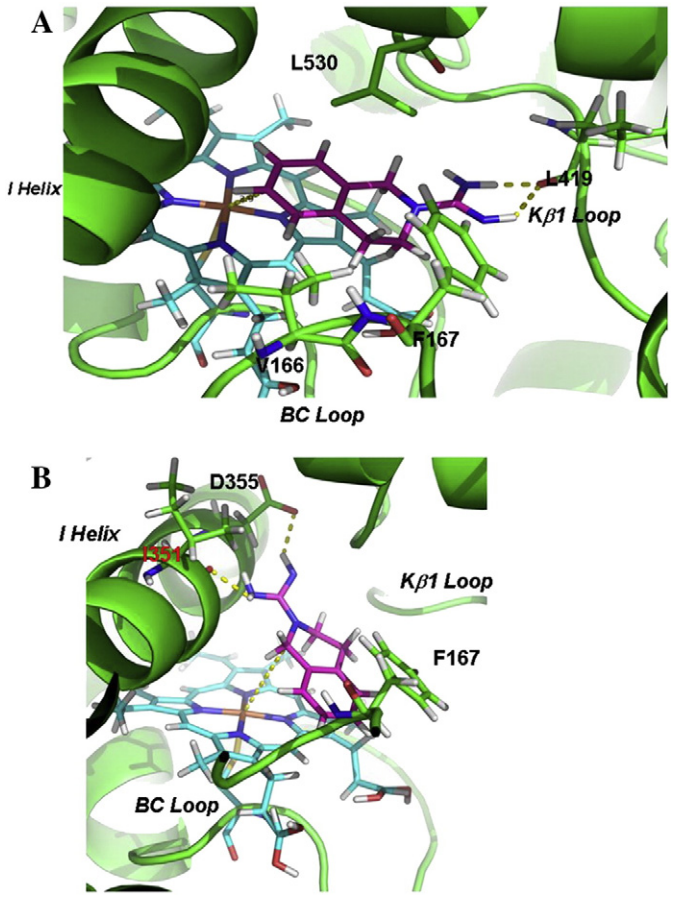

Fig. 4. 3D Model of the positioning of Deb at the active site of CYP2U1. The apoprotein is shown in green, the heme in blue and Deb in purple. A: Cluster 1 leading to the formation of 6-OH-Deb; B: Cluster 3 leading to the formation of 1-OH-Deb.

Other observed interactions concerned hydrophobic residues, with a specific role for Phe310 in π-stacking interaction with one of the terminal phenyl groups of Et-Terf [26,71]. Alignment of the sequences of CYP2J2 and CYP2U1 (Fig. S7 of the Supporting information) showed that there was no polar equivalent to Arg117 in CYP2U1, the residue corresponding to Arg117 being Ile256. This suggested that the modes of association of the Terf derivatives could greatly differ between CYP2J2 and CYP2U1. Docking of Et-Terf, **8**, in CYP2U1 was done with the method previously used in the case of Deb. The clustering of poses was obtained for a similarity threshold of 3 Å between two poses, this threshold being higher than that chosen for Deb as Terf analogues displayed a larger flexibility than Deb. Two clusters of low energy ($-9/-6$ kcal·mol^{-1}) and containing over 100 exposures were consistent with the observed regioselectivities. In the first cluster, Et-Terf was positioned along access channel S whereas it was positioned along access channel 2ac in the second cluster (Fig. 5). Other clusters corresponded to poses where the substrate was too far away from the active site. The positioning of Et-Terf within the active site of CYP2U1 differed from what was observed with CYP2J2, as the substrate chooses different access channels of these proteins. Actually, Et-Terf followed channel 2b to enter the active site of CYP2J2, whereas it followed channels S or 2ac of CYP2U1 in the two clusters of poses mentioned above (Fig. 5).

A view of the docking poses and of the corresponding interactions is shown in Fig. 6 for input by channels S and 2ac. When Et-Terf followed channel S (Fig. 6A), its aliphatic terminus (close to the heme) would interact with hydrophobic residues Val417 and Leu530 and there was a π-stacking interaction with Phe167 of loop BC. The ketone group of Et-Terf established a H-bond with the OH-group of Thr356 of helix I while the N-atom of the amine interacted with Asp355 of the same helix. The other contacts of the protein with the substrate were mainly provided by hydrophobic interactions (green in Fig. 6B). When Et-Terf followed channel 2ac (Fig. 6C) the same set of hydrophobic interactions was established between the ethyl-group of Et-Terf and Leu530 and Ala296, and π-stacking of the phenyl group of Et-Terf occurred with Phe167 of the BC loop. Furthermore, H-bonds interactions between the ketone group of Et-terf and Lys161 of the BC loop and between Asp348 of helix I and the amine function of Et-Terf were observed. Finally, in a similar way to that observed in the case of entry by channel S, the other interactions between the protein and the substrate following channel 2ac mainly consisted of hydrophobic interactions via apolar residues (Fig. 6D).

Docking of the three other Terf analogues **7**, **9** and **10** in the CYP2U1 active site showed that these molecules had binding modes and interactions with residues of the access channels very similar to those described for Et-Terf. All poses indicated one or more H-bonds between the ketone and the amine functions of the analogues and polar residues of the access channels. However, different interactions between residues in the immediate vicinity of the heme (first hydrophobic ring) and the terminal aliphatic chains of the analogues were observed. Docking of the Terf analogues within the active site showed that there was a constraint between the phenyl-alkyl moiety of the substrate and the protein residues close to the heme. The distances between the iron and each of the substrate alkyl chain carbons were measured and compared in Table 2. Their absolute values must be cautiously considered as they derive from a model. However, they were in the range of distances (4–6 Å) expected for the hydroxylation of the C–H bonds by the CYP iron-oxo species. Interestingly, the calculated Fe–C distances for a given substrate were in agreement with the regioselectivity of its hydroxylation by CYP2U1 mentioned above. In all cases, the lower values of the Fe–Cα distances (between 3.5 ± 0.2 and 4.0 ± 0.2 Å) completely corresponded to the hydroxylation regioselectivity favoring the benzylic position of all the active analogues. Similarly, the order of the measured distances (Fe–Cα < Fe–Cβ < Fe–Cγ < Fe–Cδ) was in agreement with the observed regioselectivity.

Our docking experiments of Terf analogues in the active site of CYP2U1 well agreed with the experimentally observed hydroxylation regioselectivities that strongly differed from those observed in the case of CYP2J2 which selectively oxidized the homobenzylic position of the Terf analogues [26]. They also differed from those observed in the case of CYP3A4 that is much less selective as it oxidizes both the amine function (major pathway) and the alkyl chain of the same

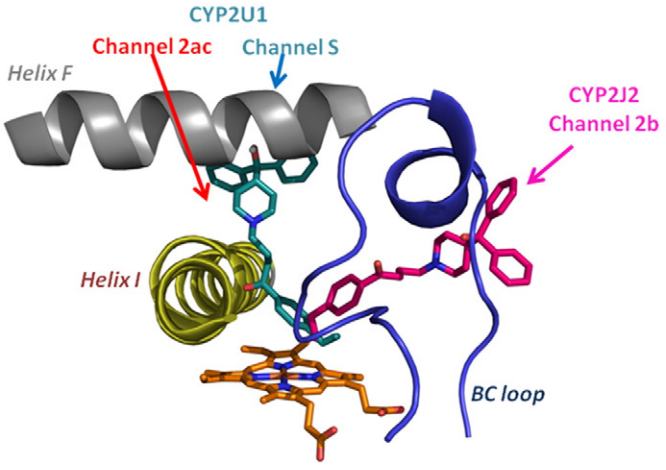

Fig. 5. Comparison of the orientations of Et-Terf within the active sites of CYP2J2 and CYP2U1. Docking of Et-Terf within the active site of CYP2J2 is shown in magenta and docking of Et-Terf within CYP2U1 is shown in blue. For the sake of clarity, only the docking pose of Et-Terf in channel S (blue arrow) is shown. Position of channel 2ac in which Et-Terf can be located is only indicated by a red arrow. Helix I, helix F and BC loop are shown in cartoon.

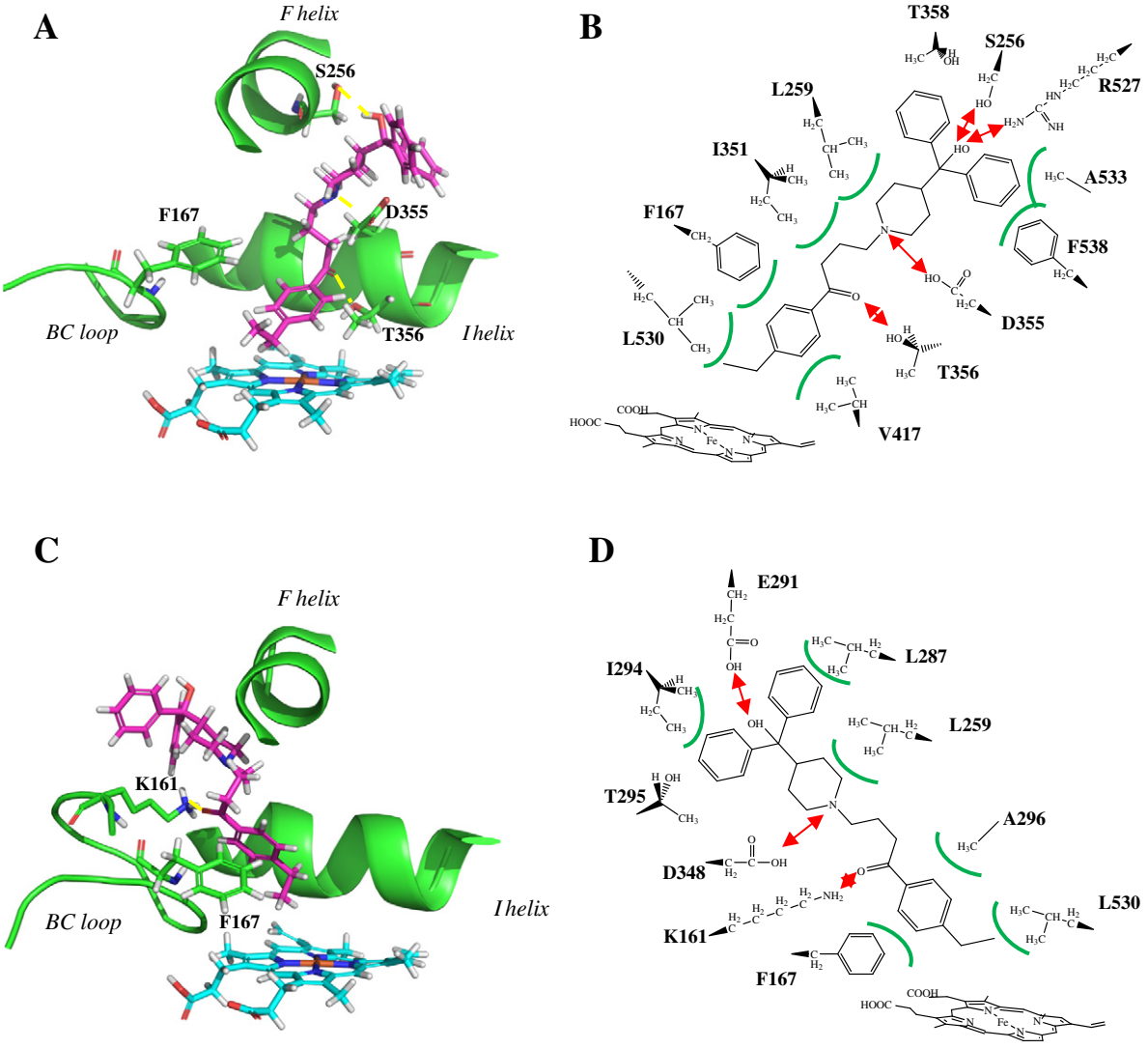

Fig. 6. 3D Model of the positioning of Et-Terf within the active site of CYP2U1 when the substrate follows channel S (A) or 2ac (C). Interactions found in the CYP2U1-Et-Terf complex when substrate follows channel S (B) or 2ac (D). The apoprotein is shown in green, the heme in blue and Et-Terf in purple. H-bonds and electrostatic interactions are shown by red arrows, and van der Waals interactions in green.

compounds [23,55]. The regioselectivity of CYP3A4 is dictated by the intrinsic chemical reactivity of the different functions of the Terf-analogues, due to the wide substrate binding site of CYP3A4. At the opposite, the highly regioselective oxidation of Terf derivatives by CYP2J2, which occurs on the poorly reactive homobenzylic C–H bonds, was attributed to a unique, very strict positioning of these substrates in its active site [26,71]. The different regioselectivities observed for Terf derivatives hydroxylation by CYP2U1 and CYP2J2 could be explained by the influence of the crown of protein residues just above the heme that leave little room for substrate access to the iron in CYP2J2 while it permits a much less constrained access in CYP2U1 (Fig. 7).

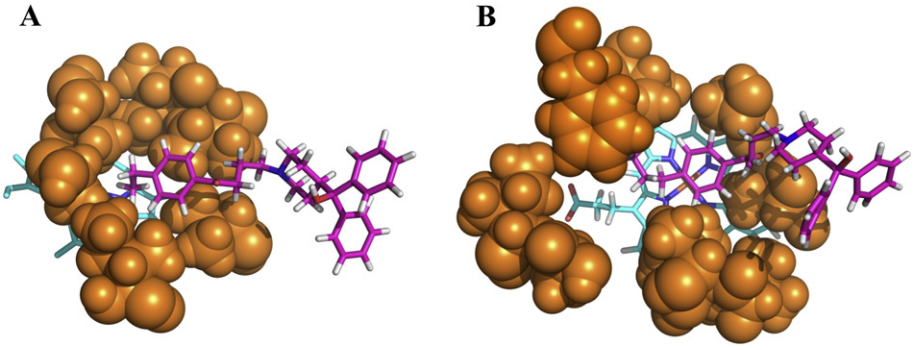

Fig. 7. Compared regioselectivity of the hydroxylation of Et-Terf in the active sites of CYP2J2 (A) and CYP2U1 (B). The amino acid residues that delineate the active site near the heme are shown in orange van der Waals spheres; Et-Terf and heme are shown as sticks.

Binding of Deb to CYP2U1 appears to be mainly due to interactions with residues in close proximity of the heme. By contrast, binding of Terf analogues should be mainly governed by their interactions with residues into the access channels.

4. Conclusion

The aforementioned results describe an efficient system for the expression of catalytically active orphan human CYP2U1 in a yeast strain, W(hR), co-expressing human CYP reductase, and a first 3D homology model of CYP2U1. A first validation of this model was obtained from docking experiments with arachidonic acid that explained the particular regioselectivity previously reported for the hydroxylation of this substrate (ω and ω-1 positions). The use of CYP2U1 expressed in W(hR) for the search of CYP2U1 substrates led, after testing a series of molecules, generally known to be transformed by other members of the CYP2 family, to the discovery of the first xenobiotic substrates of this cytochrome, Deb, an usual substrate of CYP2D6, and Terf derivatives that have been described as CYP2J2 substrates. Interestingly, the regioselectivity of CYP2U1-catalyzed hydroxylation of Deb, with the predominant formation of 1-OH-Deb, differs from that known for CYP2D6 (major formation of 4-OH-Deb). Moreover, Terf derivatives are mainly hydroxylated by CYP2U1 at their most reactive benzylic position, whereas they are predominantly hydroxylated at their homobenzylic position by CYP2J2. Molecular docking of AA and these substrates in the 3D homology model of CYP2U1 allowed us to explain the particular regioselectivities of their CYP2U1-catalyzed hydroxylations on the basis of their interactions with key residues of the active site (Figs. **3**, **4**, and **6**).

Our results show for the first time that human orphan CYP2U1 can oxidize several exogenous molecules including drugs. This could have consequences for the metabolism of drugs particularly in the brain in which CYP2U1 is mainly located. The above described docking experiments of several substrates, that exhibit quite different structures (AA, Deb and four Terf derivatives), on the CYP2U1 3D model allowed us to explain all the hydroxylation regioselectivities observed experimentally. Altogether these data provide a reasonable validation of our 3D model. This model should help the discovery of better, more selective substrates and/or inhibitors of CYP2U1. It should also be useful to identify other possible endogenous molecules as substrates of CYP2U1 and should help understanding the physiological roles of this human orphan cytochrome P450.

Acknowledgements

The authors thank Drs P. Dansette and M.A. Sari (UMR 8601 CNRS, Paris), and Dr M. Delaforge and A. Barrand-Frelet (UMR 9198 CNRS, Gif sur Yvette) for fruitful discussions. They thank Drs J.P. Flinois and C. Marchetti (UMR S 775, INSERM, Paris), M. Jaouen (UMR 8601 CNRS, Paris) and Dr P. Simon (Collège de France, Paris) for technical assistance. They thank Dr O. Laprévote (EA4463, Université Paris Descartes) and A. Hessani (UMR 8601 CNRS, Paris) for HPLC-MS studies. The authors gratefully acknowledge Dr M. Ingelman-Sundberg (Institute of Environmental Medicine Karolinska Instituet, Stockholm, Sweden) for a gift of anti-CYP2U1 antibody and Dr E. Gillam (University of Queensland, Australia) for personal communications. The authors thank the French "Ministère de l'Education et de la Recherche" for a fellowship to L.D.s and University Paris Descartes for a collaborative grant.

Appendix A. Supplementary data

Synthesis and characterization of Deb metabolites.

Expression and characterization of CYP2U1 in yeast.

PDF file of coordinates of the CYP2U1-arachidonic complex in the 3D model.

Supplementary data to this article can be found online at http://dx.doi.org/10.1016/j.bbagen.2015.03.014

References

[1] P.R. Ortiz de Montellano, Cytochrome P450: Structure, Mechanism and Biochemistry, Third editionKluwer Academic/Plenum Publishers, New York, 2005.
[2] F.P. Guengerich, Human cytochrome P450 enzymes, in: P.R. Ortiz de Montellano (Ed.), Cytochrome P450: Structure, Mechanism and Biochemistry, Third editionKluwer Academic/Plenum Publishers, New York 2005, pp. 377–530.
[3] F.P. Guengerich, Q. Cheng, Orphans in the human cytochrome P450 superfamily: approaches to discovering functions and relevance in pharmacology, Pharmacol. Rev. 63 (2011) 684–699.
[4] M. Karlgren, S. Miura, M. Ingelman-Sundberg, Novel extrahepatic cytochrome P450s, Toxicol. Appl. Pharmacol. 207 (2005) 57–61.
[5] M. Karlgren, M. Backlund, I. Johansson, M. Oscarson, M. Ingelman-Sundberg, Characterization and tissue distribution of a novel human cytochrome P450-CYP2U1, Biochem. Biophys. Res. Commun. 315 (2004) 679–685.
[6] S.S. Chuang, C. Helvig, M. Taimi, H.A. Ramshaw, A.H. Collop, M. Amad, J.A. White, M. Petkovich, G. Jones, B. Korczak, CYP2U1, a novel human thymus- and brain-specific cytochrome P450, catalyzes omega- and (omega-1)-hydroxylation of fatty acids, J. Biol. Chem. 279 (2004) 6305–6314.
[7] A. Kubota, J.J. Stegeman, J.V. Goldstone, D.R. Nelson, E.Y. Kim, S. Tanabe, H. Iwata, Cytochrome P450 CYP2 genes in the common cormorant: evolutionary relationships with 130 diapsid CYP2 clan sequences and chemical effects on their expression, Comp. Biochem. Physiol. C: Toxicol. Pharmacol. 153 (2011) 280–289.
[8] J.V. Goldstone, A.G. McArthur, A. Kubota, J. Zanette, T. Parente, M.E. Jönsson, D.R. Nelson, J.J. Stegeman, Identification and developmental expression of the full complement of cytochrome P450 genes in zebrafish, BMC Genomics 11 (2010) 643–663.
[9] F. Dutheil, S. Dauchy, M. Diry, V. Sazdovitch, O. Cloarec, L. Mellottée, I. Bièche, M. Ingelman-Sundberg, J.P. Flinois, I. de Waziers, P. Beaune, X. Declèves, C. Duyckaerts, M.A. Loriot, Xenobiotic-metabolizing enzymes and transporters in the normal human brain: regional and cellular mapping as a basis for putative roles in cerebral function, Drug Metab. Dispos. 37 (2009) 1528–1538.
[10] A. Devos, C.L. Lino Cardenas, F. Glowacki, A. Engels, J.M. Lo-Guidice, D. Chevalier, D. Allorge, F. Broly, C. Cauffiez, Genetic polymorphism of CYP2U1, a cytochrome P450 involved in fatty acids hydroxylation, Prostaglandins Leukot. Essent. Fat. Acids 83 (2010) 105–110.
[11] R. Shawahna, Y. Uchida, X. Declèves, S. Ohtsuki, S. Yousif, S. Dauchy, A. Jacob, F. Chassoux, C. Daumas-Duport, P.O. Couraud, T. Terasaki, J.M. Scherrmann, Transcriptomic and quantitative proteomic analysis of transporters and drug metabolizing enzymes in freshly isolated human brain microvessels, Mol. Pharm. 8 (2011) 1332–13341.
[12] X. Decleves, A. Jacob, S. Yousif, R. Shawahna, S. Potin, J.M. Scherrmann, Interplay of drug metabolizing CYP450 enzymes and ABC transporters in the blood–brain barrier, Curr. Drug Metab. 12 (2011) 732–741.
[13] I. Bièche, C. Narjoz, T. Asselah, S. Vacher, P. Marcellin, R. Lidereau, P. Beaune, I. de Waziers, Reverse transcriptase-PCR quantification of mRNA levels from cytochrome (CYP)1, CYP2 and CYP3 families in 22 different human tissues, Pharmacogenet. Genomics 17 (2007) 731–742.
[14] S. Ellero, G. Chakhtoura, C. Barreau, S. Langouët, C. Benelli, L. Penicaud, P. Beaune, I. de Waziers, Xenobiotic-metabolizing cytochromes P450 in human white adipose tissue: expression and induction, Drug Metab. Dispos. 38 (2010) 679–686.
[15] Y.B. Jarrar, S.A. Cho, K.S. Oh, D.H. Kim, J.G. Shin, S.J. Lee, Identification of cytochromes P450s involved in the metabolism of arachidonic acid in human platelets, Prostaglandins Leukot. Essent. Fat. Acids 89 (2013) 227–234.
[16] G.I. Murray, S. Patimalla, K.N. Stewart, I.D. Miller, S.D. Heys, Profiling the expression of cytochrome P450 in breast cancer, Histopathology 57 (2010) 202–211.
[17] M. Kumarakulasingham, P.H. Rooney, S.R. Dundas, C. Telfer, W.T. Melvin, S. Curran, G.I. Murray, Cytochrome P450 profile of colorectal cancer: identification of markers of prognosis, Clin. Cancer Res. 11 (2005) 3758–3765.
[18] C. Tesson, M. Nawara, M.A. Salih, R. Rossignol, M.S. Zaki, M. Al Balwi, R. Schule, C. Mignot, E. Obre, A. Bouhouche, F.M. Santorelli, C.M. Durand, A.C. Oteyza, K.H. El-Hachimi, A. Al Drees, N. Bouslam, F. Lamari, S.A. Elmalik, M.M. Kabiraj, M.Z. Seidahmed, T. Esteves, M. Gaussen, M.L. Monin, G. Gyapay, D. Lechner, M. Gonzalez, C. Depienne, F. Mochel, J. Lavie, L. Schols, D. Lacombe, M. Yahyaoui, I. Al Abdulkareem, S. Zuchner, A. Yamashita, A. Benomar, C. Goizet, A. Durr, J.G. Gleeson, F. Darios, A. Brice, G. Stevanin, Alteration of fatty-acid-metabolizing enzymes affects mitochondrial form and function in hereditary spastic paraplegia, Am. J. Hum. Genet. 91 (2013) 1051–1064.
[19] M. Siller, S. Goyal, F.K. Yoshimoto, Y. Xiao, S. Wei, F.P. Guengerich, Oxidation of endogenous *N*-arachidonoylserotonin by human cytochrome P450 2U1, J. Biol. Chem. 289 (2014) 10476–10487.
[20] M.H. Luria, E.D. Freis, Treatment of hypertension with debrisoquine sulfate (Declinax), Curr. Ther. Res. Clin. Exp. 7 (1965) 289–296.
[21] T. Kronbach, Bufuralol, dextromethorphan, and debrisoquine as prototype substrates for human P450IID6, Methods Enzymol. 206 (1991) 509–517.
[22] T. Lightfoot, S.W. Ellis, J. Mahling, M.J. Ackland, F.E. Blaney, G.J. Bijloo, M.J. De Groot, N.P. Vermeulen, G.M. Blackburn, M.S. Lennard, G.T. Tucker, Regioselective hydroxylation of debrisoquine by cytochrome P4502D6: implications for active site modelling, Xenobiotica 30 (2000) 219–233.
[23] C.H. Yun, R.A. Okerholm, F.P. Guengerich, Oxidation of the antihistaminic drug terfenadine in human liver microsomes. Role of cytochrome P-450 3A(4) in N-dealkylation and C-hydroxylation, Drug Metab. Dispos. 21 (1993) 403–409.

[24] P. Lafite, S. Dijols, D. Buisson, A.C. Macherey, D.C. Zeldin, P.M. Dansette, D. Mansuy, Design and synthesis of selective, high-affinity inhibitors of human cytochrome P450 2J2, Bioorg. Med. Chem. Lett. 16 (2006) 2777–2780.
[25] P. Lafite, S. Dijols, D.C. Zeldin, P.M. Dansette, D. Mansuy, Selective, competitive and mechanism-based inhibitors of human cytochrome P450 2J2, Arch. Biochem. Biophys. 464 (2007) 155–168.
[26] P. Lafite, F. André, D.C. Zeldin, P.M. Dansette, D. Mansuy, Unusual regioselectivity and active site topology of human cytochrome P450 2J2, Biochemistry 46 (2007) 10237–10247.
[27] M.S. Bernatowicz, Y. Wu, G.R. Matsueda, Urethane protected derivatives of 1-Guanylpyrazole for the mild and efficient preparation of guanidines, Tetrahedron Lett. 34 (1993) 3389–3392.
[28] B.R. Cooke, S.W.A. Bligh, Z.R. Cybulski, C. Ioannides, M. Hall, Debrisoquine metabolism and CYP2D expression in marmoset liver microsomes, Drug Metab. Dispos. 40 (2012) 70–75.
[29] D. Pompon, B. Louerat, A. Bronine, P. Urban, Yeast expression of animal and plant P450s in optimized redox environments, Methods Enzymol. 272 (1996) 51–64.
[30] P. Urban, G. Truan, J.C. Gautier, D. Pompon, Xenobiotic metabolism in humanized yeast: engineered yeast cells producing human NADPH-cytochrome P-450 reductase, cytochrome b5, epoxide hydrolase and P-450s, Biochem. Soc. Trans. 21 (1993) 1028–1034.
[31] M.A. Peyronneau, J.P. Renaud, G. Truan, P. Urban, D. Pompon, D. Mansuy, Optimization of yeast-expressed human liver cytochrome P450 3A4 catalytic activities by coexpressing NADPH-cytochrome P450 reductase and cytochrome b_5, Eur. J. Biochem. 207 (1992) 109–116.
[32] M.M. Bradford, A rapid and sensitive method for the quantitation of microgram quantities of protein utilizing the principle of protein-dye binding, Anal. Biochem. 72 (1976) 248–254.
[33] F.P. Guengerich, M.V. Martin, C.D. Sohl, Q. Cheng, Measurement of cytochrome P450 and NADPH cytochrome P450 reductase, Nat. Protoc. 4 (2009) 1245–1251.
[34] A. Sali, L. Potterton, F. Yuan, H. Vanvlijmen, M. Karplus, Evaluation of comparative protein modeling by modeller, Proteins 23 (1995) 318–326.
[35] R.A. Laskowski, M.W. Macarthur, D.S. Moss, J.M. Thornton, Procheck — a program to check the stereochemical quality of protein structures, J. Appl. Crystallogr. 26 (1993) 283–291.
[36] R.W. Hooft, G. Vriend, C. Sander, E.E. Abola, Errors in protein structures, Nature 381 (1996) 272.
[37] C. Colovos, T.O. Yeates, Verification of protein structures: patterns of nonbonded atomic interactions, Protein Sci. 2 (1993) 1511–1519.
[38] J.U. Bowie, R. Luthy, D. Eisenberg, A method to identify protein sequences that fold into a known three-dimensional structure, Science 253 (1991) 164–170.
[39] D.A. Case, T.E. Cheatham, T. Darden, H. Gohlke, R. Luo, K.M. Merz, A. Onufriev, C. Simmerling, B. Wang, R.J. Woods, The Amber biomolecular simulation programs, J. Comput. Chem. 26 (2005) 1668–1688.
[40] A. Oda, N. Yamaotsu, S. Hirono, New AMBER force field parameters of heme iron for cytochrome P450s determined by quantum chemical calculations of simplified models, J. Comput. Chem. 26 (2005) 818–826.
[41] K. Shahrokh, A. Orendt, G.S. Yost, T.E. Cheatham, Quantum mechanically derived AMBER-compatible heme parameters for various states of the cytochrome P450 catalytic cycle, J. Comput. Chem. 33 (2012) 119–133.
[42] G.J. Kleywegt, T.A. Jones, Detection, delineation, measurement and display of cavities in macromolecular structures, Acta Crystallogr. Sect. D: Biol. Crystallogr. 50 (1994) 178–185.
[43] M. Petrek, P. Kosinova, J. Koca, M. Otyepka, MOLE: a Voronoi diagram-based explorer of molecular channels, pores, and tunnels, Structure 15 (2007) 1357–1363.
[44] D.S. Goodsell, G.M. Morris, A.J. Olson, Automated docking of flexible ligands: applications of AutoDock, J. Mol. Recognit. 9 (1996) 1–5.
[45] G.M. Morris, R. Huey, W. Lindstrom, M.F. Sanner, R.K. Belew, D.S. Goodsell, A.J. Olson, AutoDock4 and AutoDockTools4: automated docking with selective receptor flexibility, J. Comput. Chem. 30 (2009) 2785–2791.
[46] G. Wu, D.H. Robertson, C.L. Brooks, M. Vieth, Detailed analysis of grid-based molecular docking: a case study of CDOCKER — a CHARMm-based MD docking algorithm, J. Comput. Chem. 24 (2003) 1549–1562.
[47] J.G. Allen, P.B. East, R.J. Francis, J.L. Haigh, Metabolism of debrisoquine sulfate. Identification of some urinary metabolites in rat and man, Drug Metab. Dispos. 3 (1975) 332–337.
[48] P.M. Cerqueira, F.H. Mateus, E.J. Cesarino, P.S. Bonato, V.L. Lanchote, Enantioselectivity of debrisoquine 4-hydroxylation in Brazilian Caucasian hypertensive patients phenotyped as extensive metabolizers, J. Chromatogr. B 749 (2000) 153–161.
[49] M. Eichelbaum, M. Bertilsson, A. Küpfer, E. Steiner, C.O. Meese, Enantioselectivity of 4-hydroxylation in extensive and poor metabolizers of debrisoquine, Br. J. Clin. Pharmacol. 25 (1988) 505–508.
[50] Y. Zhen, O. Slanar, K.W. Krausz, C. Chen, J. Slavík, K.L. McPhail, T.M. Zabriskie, F. Perlík, F.J. Gonzalez, J.R. Idle, 3,4-Dehydrodebrisoquine, a novel debrisoquine metabolite formed from 4-hydroxydebrisoquine that affects the CYP2D6 metabolic ratio, Drug Metab. Dispos. 34 (2006) 1563–1574.
[51] B. Eiermann, P.O. Edlund, A. Tjernberg, P. Dalén, M.L. Dahl, L. Bertilsson, 1- and 3-hydroxylations, in addition to 4-hydroxylation, of debrisoquine are catalyzed by cytochrome P450 2D6 in humans, Drug Metab. Dispos. 26 (1998) 1096–1101.
[52] T. Hiroi, T. Chow, S. Imaoka, Y. Funae, Catalytic specificity of CYP2D isoforms in rat and human, Drug Metab. Dispos. 30 (2002) 970–976.
[53] B. Clement, M.H. Schultze-Mosgau, H. Wohlers, Cytochrome P450 dependent *N*-hydroxylation of a guanidine (debrisoquine), microsomal catalysed reduction and further oxidation of the *N*-hydroxy-guanidine metabolite to the urea derivative. Similarity with the oxidation of arginine to citrulline and nitric oxide, Biochem. Pharmacol. 46 (1994) 2249–2267.
[54] M.A. Correia, P.R. Ortiz de Montellano, Inhibition of cytochrome P450 enzymes, in: P.R. Ortiz de Montellano (Ed.), Cytochrome P450: Structure, Mechanism, and Biochemistry, Third editionKluwer Academic/Plenum Publishers, New York 2005, pp. 247–322.
[55] K.H.J. Ling, G.A. Leeson, S.D. Burmaster, R.H. Hook, M.K. Reith, L.K. Cheng, Metabolism of terfenadine associated with CYP3A(4) activity in human hepatic microsomes, Drug Metab. Dispos. 23 (1995) 631–636.
[56] S.F. Altschul, T.L. Madden, A.A. Schaffer, J. Zhang, Z. Zhang, W. Miller, D.J. Lipman, Gapped BLAST and PSI-BLAST: a new generation of protein database search programs, Nucleic Acids Res. 25 (1997) 3389–3402.
[57] R.C. Edgar, MUSCLE: a multiple sequence alignment method with reduced time and space complexity, BMC Bioinf. 5 (2004) 113–131.
[58] A.S. Konagurthu, J.C. Whisstock, P.J. Stuckey, A.M. Lesk, MUSTANG: a multiple structural alignment algorithm, Proteins 64 (2006) 559–574.
[59] V. Cojocaru, P.J. Winn, R.C. Wade, The ins and outs of cytochrome P450s, Biochim. Biophys. Acta 1770 (2007) 390–401.
[60] V. Cojocaru, K. Balali-Mood, M.S.P. Sansom, R.C. Wade, Structure and dynamics of the membrane-bound cytochrome P450 2C9, PLoS Comput. Biol. 7 (2011) e1002152.
[61] G.A. Schoch, J.K. Yano, S. Sansen, P.M. Dansette, C.D. Stout, E.F. Johnson, Determinants of cytochrome P450 2C8 substrate binding. Structures of complexes with montelukast, troglitazone, felodipine and 9-*cis*-retinoic acid, J. Biol. Chem. 283 (2008) 17227–17237.
[62] M.J. de Groot, N.P. Vermeulen, J.D. Kramer, F.A. van Acker, G.M. Donné-Op den Kelder, A three-dimensional protein model for human cytochrome P450 2D6 based on the crystal structures of P450 101, P450 102, and P450 108, Chem. Res. Toxicol. 9 (1996) 1079–1091.
[63] S.W. Ellis, G.P. Hayhurst, G. Smith, T. Lightfoot, M.M. Wong, A.P. Simula, M.J. Ackland, M.J. Sternberg, M.S. Lennard, G.T. Tucker, C.R. Wolf, Evidence that aspartic acid 301 is a critical substrate-contact residue in the active site of cytochrome P450 2D6, J. Biol. Chem. 270 (1995) 29055–29058.
[64] M.J. de Groot, M.J. Ackland, V.A. Horne, A.A. Alex, B.C. Jones, Novel approach to predicting P450-mediated drug metabolism: development of a combined protein and pharmacophore model for CYP2D6, J. Med. Chem. 42 (1999) 1515–1524.
[65] S.W. Ellis, G.P. Hayhurst, T. Lightfoot, G. Smith, J. Harlow, K. Rowland-Yeo, C. Larsson, J. Mahling, C.K. Lim, C.R. Wolf, M.G. Blackburn, M.S. Lennard, G.T. Tucker, Evidence that serine 304 is not a key ligand-binding residue in the active site of cytochrome P450 2D6, Biochem. J. 345 (2000) 565–571.
[66] M.J. Paine, L.A. McLaughlin, J.U. Flanagan, C.A. Kemp, M.J. Sutcliffe, G.C. Roberts, C.R. Wolf, Residues glutamate 216 and aspartate 301 are key determinants of substrate specificity and product regioselectivity in cytochrome P450 2D6, J. Biol. Chem. 278 (2003) 4021–4027.
[67] C. de Graaf, C. Oostenbrink, P.H. Keizers, T. van der Wijst, A. Jongejan, N.P. Vermeulen, Catalytic site prediction and virtual screening of cytochrome P450 2D6 substrates by consideration of water and rescoring in automated docking, J. Med. Chem. 49 (2006) 2417–2430.
[68] R.J. Unwalla, J.B. Cross, S. Salaniwal, A.D. Shilling, L. Leung, J. Kao, C. Humblet, Using a homology model of cytochrome P450 2D6 to predict substrate site of metabolism, J. Comput. Aided Mol. Des. 24 (2010) 237–256.
[69] P. Rowland, F.E. Blaney, M.G. Smyth, J.J. Jones, V.R. Leydon, A.K. Oxbrow, C.J. Lewis, M.G. Tennant, S. Modi, D.S. Eggleston, R.J. Chenery, A.M. Bridges, Crystal structure of human cytochrome P450 2D6, J. Biol. Chem. 281 (2006) 7614–7622.
[70] A. Wang, U. Savas, M.H. Hsu, D. Stout, E.F. Johnson, Crystal structure of human cytochrome P450 2D6 with prinomastat bound, J. Biol. Chem. 287 (2012) 10834–10843.
[71] W. Li, Y. Tang, H. Liu, J. Cheng, W. Zhu, H. Jiang, Probing ligand binding modes of human cytochrome P450 2J2 by homology modeling, molecular dynamics simulation, and flexible molecular docking, Proteins Struct. Funct. Genet. 71 (2008) 938–949.